Organic Process Research & Development **2010,** *14,* 511–523

Application of ATR-UV Spectroscopy for Monitoring the Crystallisation of UV Absorbing and Nonabsorbing Molecules

Pascal Billot,* Magdalena Couty, and Patrik Hosek

Sanofi Aventis, Research and Development, Physical Quality, 94403 Vitry-sur-Seine, France

Abstract:

In the pharmaceutical industry, controlling the crystallization process of active pharmaceutical ingredients (API) is crucial to ensure chemical quality and physical properties. Process analytical technologies (PAT) provide a large number of tools that provide information in real-time to allow mastery of the final solid chain. In this paper is described how attenuated total reflection ultraviolet (ATR-UV) spectroscopy can be used to monitor concentration. Besides its classical application to UV-absorbing molecules, it will be shown how, in principle, it may be applied to molecules that do not absorb at UV wavelengths.

1. Introduction

Active pharmaceutical ingredients (API) need to comply with chemical quality specifications and must present desirable end-use properties. While chemical quality is often well controlled ahead of the final crystallization step, end-use properties rely completely on the physical characteristics induced by the solid chain, including the crystallization, filtration, and drying. For instance, API polymorphs resulting from the solid chain have distinct crystal structures, melting points, densities, and hygroscopicities and as a consequence differences in surface reactivity and bioavailability.[1] Equally, API particle size distribution (PSD) and morphology govern flowability, filtration, and dissolution rates which considerably affect both downstream processing and biophysical properties.

The development of an efficient and robust crystallization process producing a high-quality product with desirable micromeritics is crucial. This task is facilitated by obtaining real-time information on two key parameters, the concentration and supersaturation. Supersaturation, the driving force of crystallization, is generated by cooling the solution below the solubility curve. During the cooling, the solution crosses a metastable zone (MSZ) where nucleation requires a long induction time and but where crystals will grow. At the lower limit of this zone, corresponding to the unstable zone on the Ostwald−Miers diagram (Figure 1), spontaneous nucleation and then crystal growth occur, until reaching the equilibrium (solubility curve). The level of supersaturation which can be created depends on the metastable zone width (MSZW). Introducing a small amount of seed crystals inside the reactor, generally one-third of the way into the MSZW allows optimal control of the crystallization process to target a specific polymorph and/or particle size range. This generic rule of thumb should be applied with care as there is a very large difference between the MSZW based on primary nucleation and the MSZW in a seeded system. Very often organic molecules have a very large primary MSZW and a much narrower operating zone for supersaturation control in the case of seeded systems. In most cases, introducing seed at one-third of the MSZW for primary nucleation would generate instant nucleation, and thus seeding should be done much closer to the solubility curve.

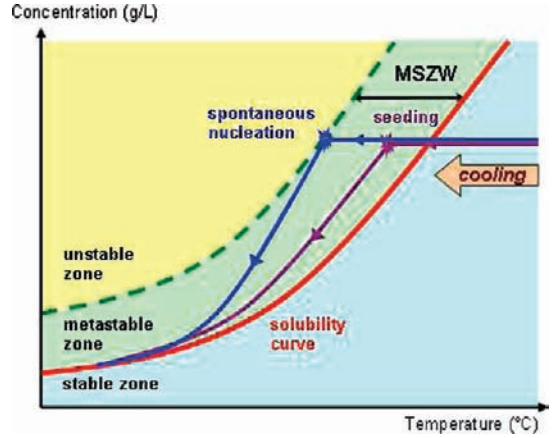

Figure 1. **Ostwald−Miers diagram.**

Real-time information on concentration is available using process analytical technologies (PAT),[2] as recommended by the U.S. Food and Drug Administration[3] since 2001, in order to understand and improve the process and avoid failed batches. While external sampling in case of at-line PAT and analysis loops in the case of on-line PAT show serious shortcomings, such as poor temperature control during the sample analysis that could alter polymorphic form or particle size, in-line PAT (probes or sensors directly in contact with material inside the reactor) minimize artefacts due to sample isolation and preparation and thus are the most desirable techniques.

Research and development efforts focusing on PAT in crystallization[4] have led to mature techniques to monitor either the liquid phase or the solid phase or possibly both phases.

* Corresponding author. E-mail: pascal.billot@sanofi-aventis.com.

(1) Byrn, S.; Pfeiffer, R.; Stowell, J. *Solid-State Chemistry of Drugs*, 2nd ed.; SSCI Inc: West Lafayette, 1999.

(2) Bakeev, K. *Process Analytical Technology*; Blackwell: Oxford, 2005.

(3) PAT - A Framework for Innovative Pharmaceutical Development, Manufacturing, and Quality Assurance, Guidance for Industry; U.S. Department of Health and Human Services, Food and Drug Administration, Center for Drug Evaluation and Research (CDER): Rockville, MD, 2004; http://www.fda.gov/downloads/Drugs/GuidanceComplianceRegulatoryInformation/Guidances/UCM070305.pdf.

(4) Barrett, P.; Smith, B.; Worlitschek, J.; Bracken, V.; O'Sullivan, B.; O'Grady, D. *Org. Process Rev. Dev.* **2005**, *9*, 348.

10.1021/op900281m
Published on Web 04/14/2010

- In the liquid phase, spectroscopic techniques such as FTIR,[5] NIR,[6] or Raman[7] are the favored choices. The sugar industry prefers refractometry for monitoring crystallization. In case of an ionic medium, conductivity measurement is an option.
- In the solid phase, polymorphism is monitored by Raman spectroscopy,[7] while particle properties are followed either by *in situ* video monitoring or by focused beam reflectance measurement (FBRM) technology[5] for morphology or particle size distribution. Turbidimetry is used to monitor dissolution/nucleation points and to gain a rough idea on the evolution of particle size/concentration.

Analysis of the liquid phase using attenuated total reflection ultraviolet (ATR-UV) spectroscopy is another potential technique for monitoring crystallization processes. The main applications of UV spectroscopy are in cleaning validation, dissolution rate testing, and reaction monitoring.[2] ATR-UV spectroscopy has also been used for quantification of hydroxide, sulfide, and carbonate in kraft liquors.[8] Publications regarding crystallization include dissolution curve determination,[9] detection of nucleation point,[10] and MSZW.[11] Others focus on real-time concentration monitoring during crystallization and the control of polymorphism and particle size uniformity,[12] or the detection of polymorphic transformation.[13] In addition this technique is potentially useful for supersaturation-controlled batch crystallization. Such an approach uses feedback control to follow a set-point supersaturation curve in the metastable zone. Supersaturation is calculated from in-process solution concentration measurements either by ATR-FTIR[14,15] or ATR-UV.[16] Advantages offered by the use of the ATR-UV probe to measure supersaturation levels and to monitor crystallization processes on-line are significant.

- The technique induces no disturbance to the equilibrium of the system during the experiment.
- The ATR probe is tolerant of particles in suspension or of bubbles, allowing measurements of slurries with high solid content.
- Most APIs have at least one chromophore so that the technique might find a wide application in the pharmaceutical industry.
- The equipment is easy to set up at laboratory and plant scale, and inexpensive compared to the cost of other PATs such as ATR-FTIR. Conformity with explosive atmosphere directives (ATEX) is possible as spectrophotometers, light sources, and computers traditionally used in the laboratory may be displaced from the industrial environment in a remote manner through the use of optic-fiber waveguides as long as 100 m.

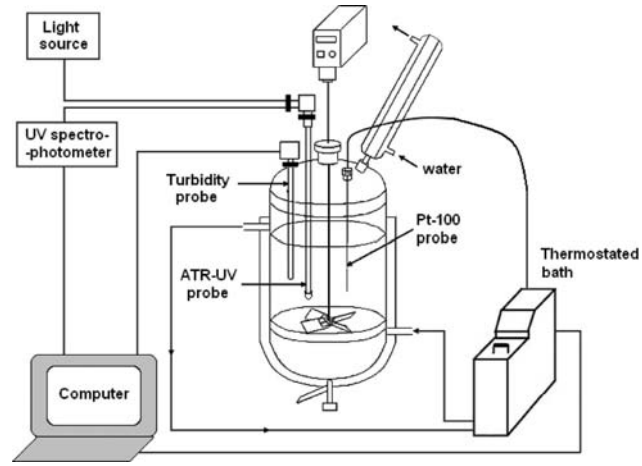

Figure 2. **Experimental setup.**

This article presents an additional contribution to the monitoring of concentration during crystallization processes by the use of ATR-UV. Application to UV-absorbing molecules is first examined. Then it is further demonstrated, at least from a theoretical point of view, that the technique may be feasible for monitoring crystallizations even for non-UV-absorbing molecules.

2. Material and Methods

The test compound was 6-methoxy-2-naphthaleneacetic acid (6-MNA), purchased from Acros Organics, Geel, Belgium. All the solvents were of analytical grade from Alfa Aesar GmbH & Co. KG, Karlsruhe, Germany.

The solubility curve and MSZW of 6-MNA in ethanol were determined using the Crystal16 system (Avantium, Amsterdam, Netherlands) which contains 4 by 4 reactor blocks of 1.5 mL HPLC vials agitated by magnetic fleas. Each block is independently electrically heated and cooled by a combination of Peltier elements and a cryostat. Each vial contains a turbidity sensor to detect dissolution and nucleation. To obtain solubility data, vials containing known concentrations of 6-MNA were cycled between 70 and 0 °C at 0.5 °C/min, finally maintaining at 0 °C for 1 h. Two cycles were performed for reproducibility.

Crystallization experiments using the ATR-UV probe were carried out in a 150 mL jacketed reactor (Figure 2). The temperature was regulated by a Huber Unistat Tango unit (VWR, Fontenay-sous-bois, France) using the software Labworldsoft (IKA Werke GmbH & Co. Staufen, Germany). The reactor was equipped with a Pt-100 probe, a turbidity probe (Anglia, Cambridgeshire, UK) connected to a transmitter Trb8300 (Mettler Toledo, Paris, France), and the ATR-UV probe (Hellma, Essex, UK). The internal reflection element was a three-bounce sapphire ATR crystal with an angle of incidence of 60°. Calibration spectra and real-time measurements of absorbance were

(5) Togkalidou, T.; Tung, H.-H.; Sun, Y.; Andrews, A.; Braatz, R. *Ind. Eng. Chem. Res.* **2004**, *43*, 6168.
(6) Févotte, G.; Calas, J.; Puel, F.; Hoff, C. *Ind. J. Pharm.* **2004**, *273*, 159.
(7) Févotte, G. *Chem. Eng. Res. Des.* **2007**, *85*, 906.
(8) Chai, X.; Danielsson, L.-G.; Yang, X.; Behm, M. *Process Contr. Qual.* **1998**, *11*, 153.
(9) Thompson, D.; Kougoulos, E.; Jones, A.; Wood-Kaczmar, M. *J. Cryst. Growth* **2005**, *276*, 230.
(10) Anderson, J.; Moore, S.; Tarczynski, F.; Walker, D. *Spectrochim. Acta, Part A* **2001**, *57*, 1793.
(11) Simon, L. L.; Nagy, Z. K.; Hungerbuhler, K. *Chem. Eng. Sci.* **2009**, *64*, 3344.
(12) Abu Bakar, M. R.; Nagy, Z. K.; Rielly, C. D. *Org. Process Res. Dev.* **2009**, *13*, 1343.
(13) Howard, K. S.; Nagy, Z. K.; Saha, B.; Roberston, A. L.; Steele, G.; Martin, D. *Cryst. Growth Des.* **2009**, *9*, 3964.
(14) Fujiwara, M.; Nagy, Z. K.; Chew, J. W.; Braatz, R. D. *J. Process Control* **2005**, *15*, 493.
(15) Nagy, Z. K.; Chew, J. W.; Fujiwara, M.; Braatz, R. D. *J. Process Control* **2008**, *18*, 399.
(16) Nagy, Z. K. *Comput. Chem. Eng.* **2009**, *33*, 1685.

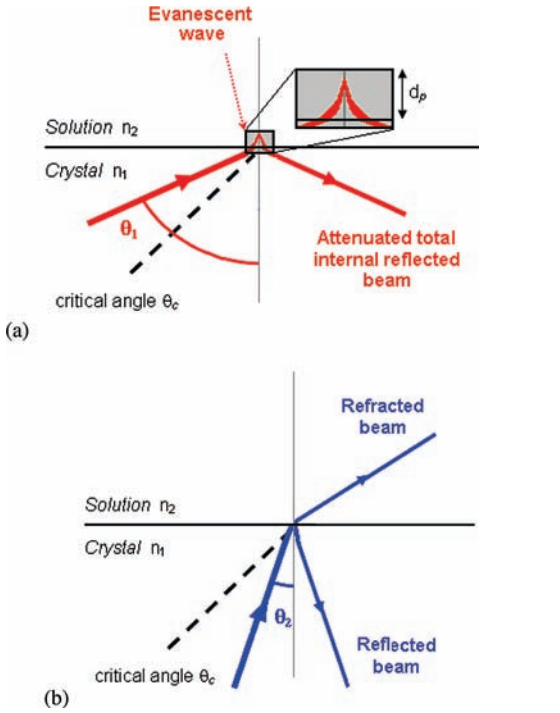

Figure 3. **Total internal reflection (a) and external reflection (b).**

recorded by the software AvaSoft provided with the single beam AvaSpec-2048 Fiber Optic Spectrophotomer (Anglia, Cambridgeshire, UK). The spectral resolution was about 1.2 nm. A calibration model was established from a statistically designed plan (DOE), using the software Nemrod (LPRAI, Marseille, France). Turbidimetry was used as a reference method to detect dissolution and nucleation points.

The particle size distribution (PSD) of isolated crystals was analyzed by the particle size analyzer Mastersizer2000 and the sample dispersion unit HydroG from Malvern Instruments Ltd., Worcestershire, UK with silicon oil as dispersant. Each sample was first submitted to ultrasound for 30 s followed by PSD measurement with a time step of 1 min, recorded under stirring at 3000 rpm The final PSD is the average of five measurements. Crystallized products were photographed using the TM-1000 tabletop microscope from Hitachi High-Technologies GmbH, Krefeld, Germany.

3. ATR−UV Theory

The principle of the attenuated total reflection probe is based on the behavior of incident radiation striking an interface between a transparent material with high refractive index n_1 (i.e., the crystal of the ATR probe) and a transparent medium with a lower refractive index n_2 (i.e., a solution). Snell's law defines a critical angle θ_c at a given wavelength (eq 1), which separates two phenomena:

- In the case of an angle of incidence θ_1 wider than θ_c (Figure 3a), an evanescent wave penetrates a path length d_p into the solution. The radiation is then completely reflected into the crystal. This phenomenon is called total internal reflection. The interaction between the evanescent wave and the species present in solution, i.e. absorption, results in an attenuation of the reflected beam.

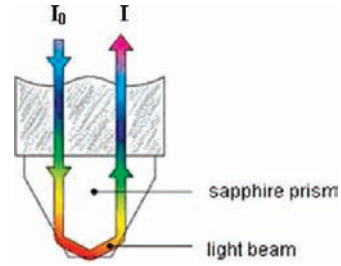

Figure 4. **Three-bounce sapphire head of the ATR probe.**

- In the case of a lower angle of incidence θ_2 (Figure 3b), the incident radiation is partially reflected and partially refracted. This phenomenon is called external reflection.

$$\theta_c(\lambda) = \arcsin\left(\frac{n_2(\lambda)}{n_1(\lambda)}\right) \quad (1)$$

For a commercial ATR device, the angle of incidence and the refractive index of the crystal n_1 are imposed by the physical characteristics of the probe (Figure 4). Thus, instead of a critical angle, one can define a critical refractive index for the solution n_{crit} (eq 2) above which total internal reflection stops and external reflection dominates. For instance, the sapphire probe used in this study with $\theta = 60°$ has an n_{crit}[20] of 1.5312 at 589 nm.

$$n_{crit} = n_1 \sin\theta \quad (2)$$

The attenuation of the reflected beam is measured as absorbance by a UV spectrophotometer. Mathematically the absorbance is defined as the logarithm of the ratio between intensities of the incident light I_0 and of the reflected light I (eq 3).

$$A = \log\left(\frac{I_0}{I}\right) \quad (3)$$

Beer−Lambert's law (eq 4) relates absorbance at a given wavelength to the concentration C of the absorbing species, the absorption coefficient ε, and the optical path length l, which for ATR-UV corresponds to the depth of penetration d_p of the evanescent wave multiplied by the number of reflections z, (i.e., 3).

$$A(\lambda) = \varepsilon(\lambda)Cl \quad (4)$$

with $l = zd_p$.

Contrary to transmission spectroscopy, in ATR spectroscopy the optical path length l is not a constant because the depth of penetration d_p of the evanescent wave into the solution is a function of the angle of incidence θ, of the wavelength λ, and of the refractive indexes n_1 and n_2 varying with temperature and wavelength.

Quantitative applications of ATR spectroscopy have been widely discussed by Müller et al.[17] They showed that a distinction must be made between absorbing and nonabsorbing media. In the case of absorbing media, the refractive index $\hat{n}$ (eq 5) is a complex number, and both the real refractive index

(17) Müller, G.; Abraham, K.; Schaldach, A. *Appl. Opt.* **1981**, *20*, 1182.

n and also the imaginary absorption index κ must be considered in calculation of d_p (eq 6).

$$\hat{n} = n + i\kappa \tag{5}$$

$$d_p = \frac{\sqrt{2}\lambda}{2\pi n_1 \sqrt{\sqrt{\mu^2 + \nu^2} - \nu}} \tag{6}$$

with

$$\mu = 2\kappa^2\left(\frac{n_2}{n_1}\right)^2, \quad \nu = \sin^2(\theta) - \left(\frac{n_2}{n_1}\right)^2(\kappa^2 - 1)$$

In the case of nonabsorbing media, κ is negligible, and the expression is simplified to eq 7.

$$d_p = \frac{\lambda}{2\pi\sqrt{(n_1)^2 \sin^2\theta - (n_2)^2}} \tag{7}$$

The depth of penetration at the critical angle increases infinitely which means that the wave propagates unattenuated into the solution. In case of absorbing media, this is no longer true, and the wave is attenuated by the absorption of sample molecules present in solution. Therefore, d_p takes a finite value.

From literature data available on the variation of refractive index with wavelength for sapphire, water,[18] toluene, and chloroform[19] (Figure 5a) and with temperature for sapphire,[20] water, ethanol, and toluene[21] (Figure 5c), d_p's were calculated using eq 7 for these solvents. Results are shown in Figure 5b,d.

Variation of the refractive index of sapphire with temperature is negligible. The limit value of refractive index is reached at 195 nm for chloroform and at 319 nm for toluene. The depth of penetration in the UV visible range is only a few micrometers and thus makes this technique suitable for direct measurements on strongly absorbing solutions where standard transmission probes cannot be used.

For qualitative and quantitative measurements by transmission with an optical path length of 1 cm, two cut-off wavelengths, with absorbance lower than 1, L_0, and with absorbance lower than 0.05, L_1, are respectively defined.[22] ATR spectra of solvents were recorded (Figure 6), and the observed cut-off wavelengths are listed in Table 1.

For solvents with a refractive index lower than 1.48, shorter cut-off wavelengths were found than those seen in transmission. Solvents showing the highest benefits in cut-off are in red bold in Table 1. In the case of ketones, it is shifted from approximately 330 nm to below 190 nm. ATR-UV spectroscopy thus allows the use of a larger number of solvents than transmission spectroscopy, a great advantage in the

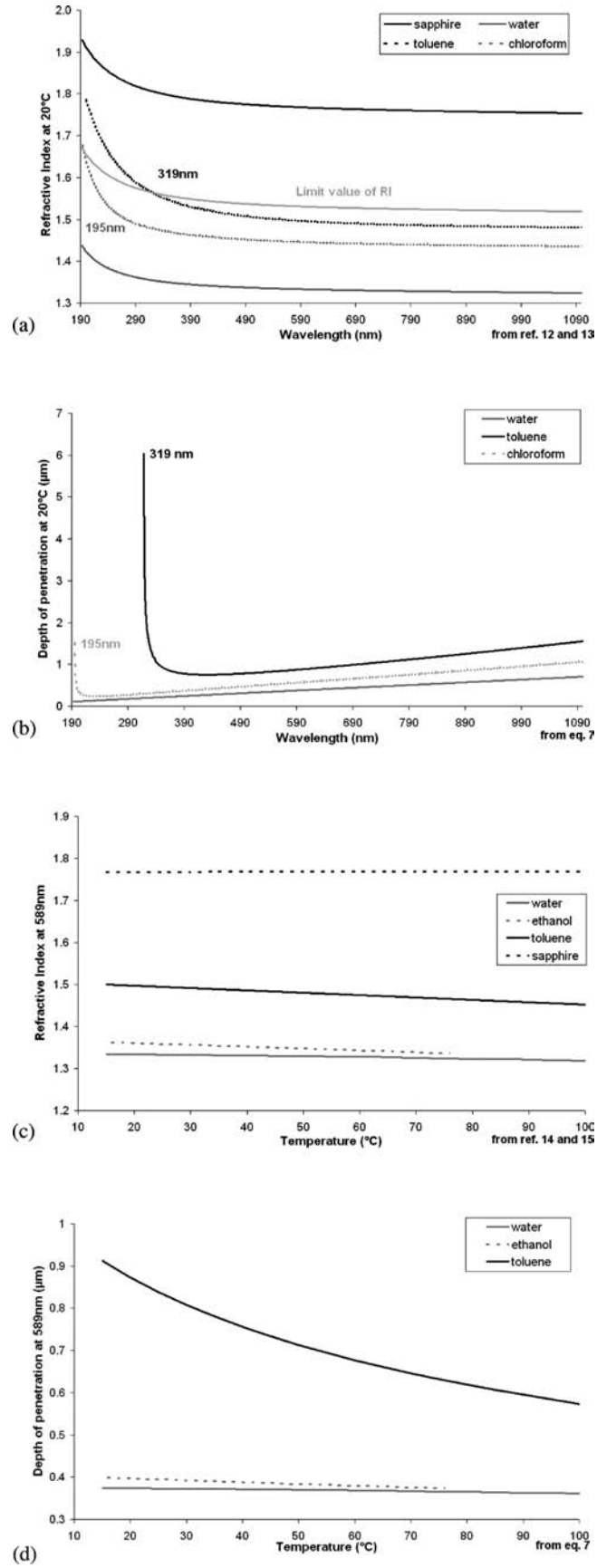

Figure 5. **Variation of refractive index (a) with wavelength at 20 °C for sapphire, water, toluene, and chloroform, and depth of penetration (b) calculated using eq 7; variation of refractive index (c) with temperature at 589 nm for sapphire, water, ethanol, and toluene, and depth of penetration (d) calculated using eq 7.**

(18) Schiebener, P.; Straub, J.; Levelt Sengers, J. M. H.; Gallagher, J. *J. Phys. Chem. Ref. Data* **1990**, *19*, 677.
(19) Samoc, A. *J. Appl. Phys.* **2003**, *94*, 6167.
(20) Bukatyj, V.; Goncharov Yu, V.; Krasnopevtsev, V. *Opt. Spektrosk.* **1984**, *56*, 461.
(21) Rubio, J.; Arsuaga, J.; Taravillo, M.; Baonza, V.; Cáceres, M. *Exp. Therm. Fluid. Sci.* **2004**, *28*, 887.
(22) Kaye and Laby Tables of Physical and Chemical Constants, web edition; National Physical Laboratory: London, UK; http://www.kayelaby.npl.co.uk/chemistry/3_8/3_8_7.html.
(23) Burdick & Jackson solvents: http://macro.lsu.edu/HowTo/solvents/UV%20Cutoff.htm.

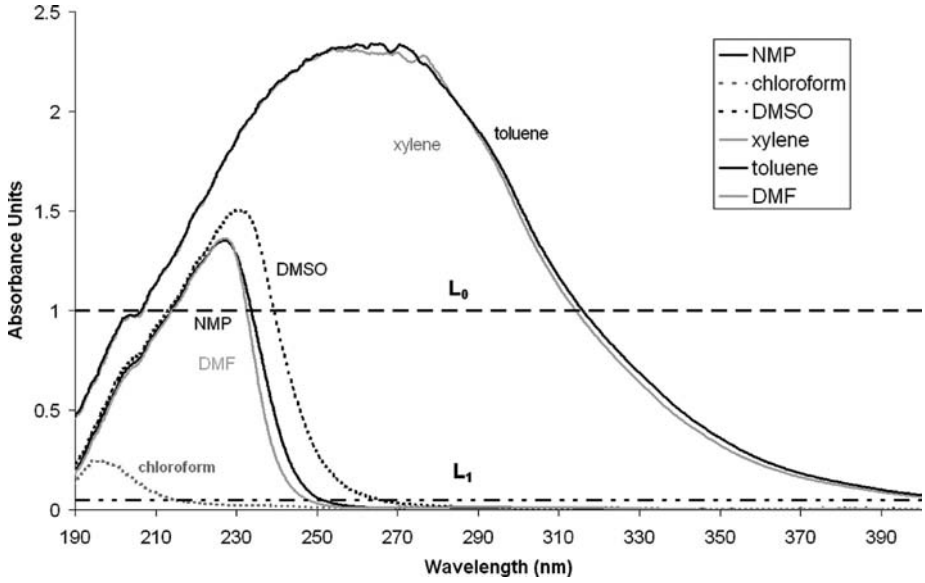

Figure 6. **ATR-UV spectra of toluene, xylene, DMSO, NMP, DMF, and chloroform.**

Table 1. **Observed and literature (from ref 22) solvents' cut-off wavelengths; reference is water**

Cut-off (nm)		Ref. 16 (Transmission)		Results (ATR)	
Solvent	n_D^{20}	L_0	L_1	L_0	L_1
methanol	1.3284	205	240	<190	<190
acetonitrile	1.3441	190	200	<190	<190
ethyl acetate	**1.3524**	**260**	**280**	**<190**	**<190**
acetone	**1.3586**	**330**	**340**	**<190**	**<190**
ethanol	1.3614	205	240	<190	<190
methyl tertiobutyl ether (MTBE)	1.3689	210 [a]	n.d. [b]	<190	<190
isopropanol	1.3772	210	250	<190	<190
methyl ethyl ketone (MEK)	**1.3788**	**330**	**345**	**<190**	**195**
n-propanol	1.3856	205	240	<190	<190
heptane	1.3876	200	230	<190	<190
methyl isobutyl ketone (MIBK)	**1.3957**	**335**	**375**	**<190**	**201**
tetrahydrofurane (THF)	1.4072	220	280	<190	196
1,4-dioxane	1.4224	220	290	<190	201
methylene chloride	1.4241	230	245	<190	203
cyclohexane	1.4262	200	235	<190	<190
dimethylformamide (DMF)	**1.4305**	**270**	**300**	**233**	**248**
chloroform	**1.4458**	**245**	**260**	**<190**	**215**
N-methylpyrrolidone (NMP)	1.4700	285 [a]	n.d. [b]	235	251
dimethylsulfoxide (DMSO)	1.4793	285	330	239	265
toluene	**1.4969**	**285**	**315**	**317**	**>400**
***o*-xylene**	**1.5054**	**290**	**325**	**311**	**390**
chlorobenzene	**1.5248**	**285**	**310**	**391**	**>750**
***o*-dichlorobenzene**	**1.5514**	**295**	**350**	**>750**	**>750**

[a] Data from Burdick and Jackson.[23] [b] n.d.= not determined.

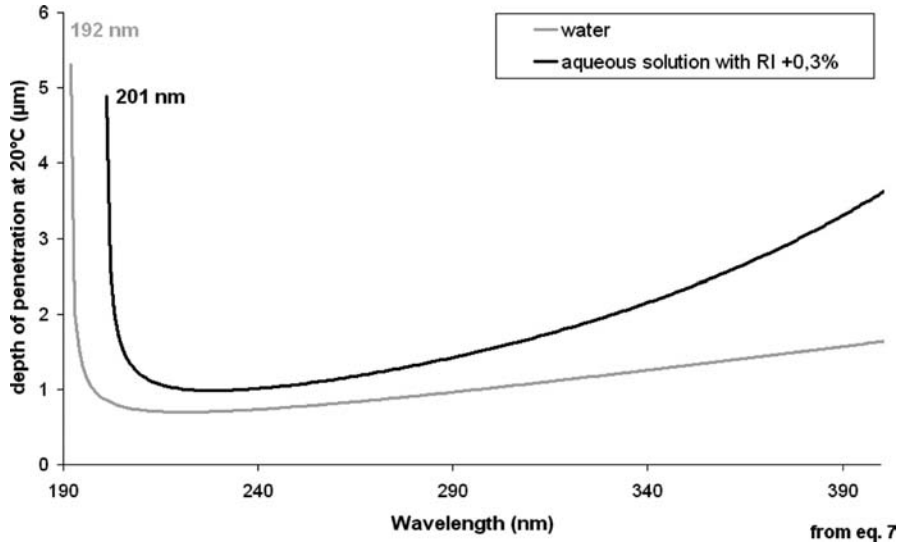

Figure 7. **Calculated d_p, using eq 7, at 20 °C with quartz as crystal, for water and for an aqueous solution of nonabsorbing substance with an increase in refractive index of 0.3%.**

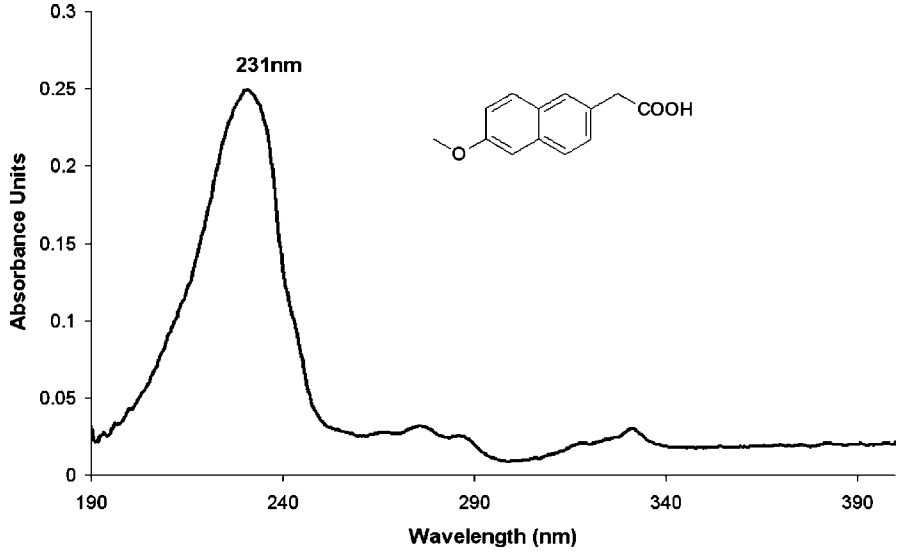

Figure 8. **Spectrum of 6-MNA 20 g/L in ethanol at 0 °C.**

crystallization field. For solvents with a refractive index higher than 1.48, and thus close to n_{crit} (in blue bold in Table 1), cut-off wavelengths were longer than for the transmission method. The cut-off observed for chloroform and toluene are in agreement with the calculated wavelengths at which n_{crit} is reached.

As the ATR technique is not only based on absorption of the sample but also on its refractive index, quantification of non-UV-absorbing molecules is possible. Indeed, a nonabsorbing molecule dissolved in a solvent with a refractive index significantly different from that of the solute and close to n_{crit}, will induce a variation in the refractive index proportional to its concentration, and will shift the cut-off wavelength. Müller et al.[17] showed with a variable-angle ATR probe that, when approaching the critical angle, the concentration of glucose in water can be measured. With quartz ($n_D^{20} = 1.5443$) as an internal reflection element and an angle of 60°, the critical refractive index becomes $n_{crit}^{20} = 1.3374$ at 589 nm and is suitable for quantitative measurements of nonabsorbing substances dissolved in water. The technique is extremely sensitive, and changes as small as $\Delta n = 0.0001$ can be detected. Using eq 7, calculation shows that an increase of 0.3% in the refractive index caused by a given concentration of a nonabsorbing substance in water will detectably shift the cut-off wavelength from 192 to 201 nm (Figure 7).

As most nonabsorbing molecules at usual solubilities induce a greater variation in refractive index than 0.3%, this technique seems, in principle, viable for non-UV-absorbing substances under certain conditions. Each couple solvent/solute requires a probe tip material with a specific refractive index to fit the n_{crit} requirement, but such a material transparent in the UV range is not often available.

4. Results and Discussion

4.1. Choice of the Test Compound. To demonstrate the ability of ATR-UV spectroscopy to monitor crystallization

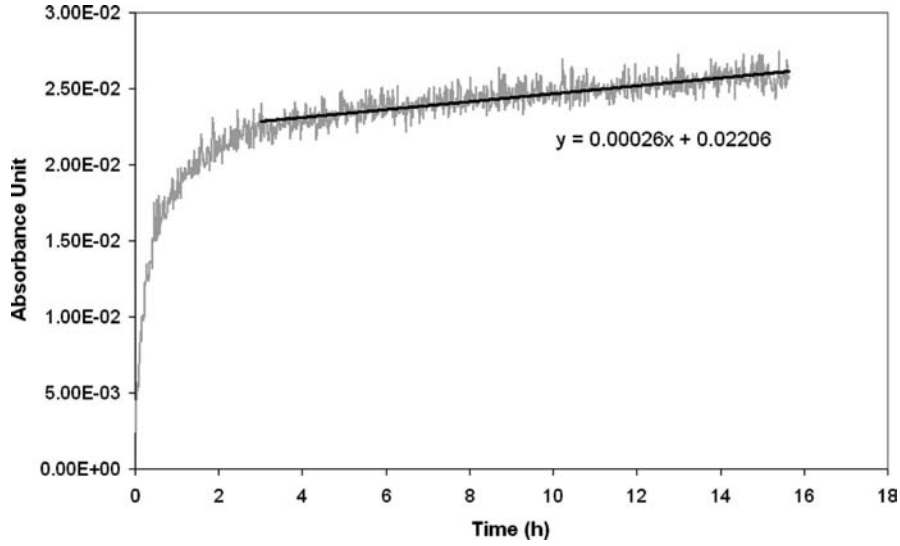

Figure 9. **Drift at 230 nm.**

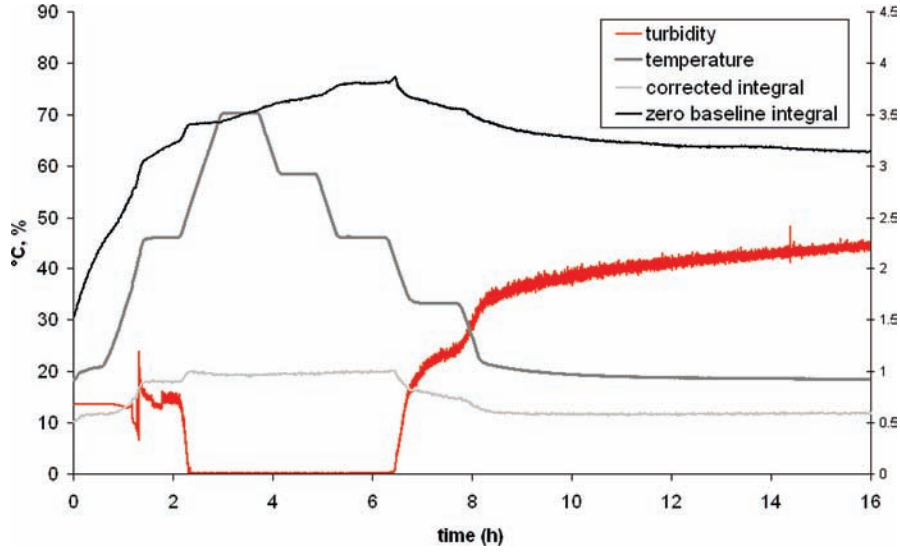

Figure 10. **Effect of baseline correction on drift.**

processes, 6-methoxy-2-naphthaleneacetic acid (6-MNA) was chosen. This compound has a naphthalene chromophore that absorbs strongly in the UV range at 231 nm (Figure 8). Amongst the solvents in which this substrate has acceptable solubility, ethanol 55 g/L, DMSO 24 g/L, and DMF 25 g/L, only ethanol is sufficiently transparent in the spectral zone of interest. Thus, the 6-MNA/ethanol system was used for further study.

4.2. In Situ UV Monitoring. Spectrophotometric techniques are subject to drift. When using a single beam UV spectrophotometer this signal stability over time should be assessed. Absorbance of ethanol was monitored at 230 nm (Figure 9) starting from the switching-on of the UV lamp up to 16 h. In order to achieve a stable drift the UV lamp should be switched on at least 3 h before in situ monitoring. The measured value of 2.6×10^{-4} AU/h will not have a big impact when working above 0.2 absorbance units (a maximum of 1% over 10 h). Under 0.2 AU it is preferable to correct the drift by subtraction of absorbance taken at another wavelength. As drift is wavelength dependent it will not be totally suppressed but rather minimized.

The same correction should be applied when peak integrals are used instead of peak heights. For monitoring dissolution and crystallization for another compound (Figure 10) with absorbance largely under 0.1, peak integration between 250 and 300 nm was preferred so as to obtain a higher signal value. During the initial 20 °C step, the UV lamp was not stabilized, and a big drift was visible on the zero baseline integral. Drift decreased over time but remained largely above 2% AU/h. When integrals are corrected for baseline (integral minus the area below a straight line between outputs at 250 and 300 nm), drift is quasi-null even during initial lamp stabilization. It should be noted that there is no hysteresis: the final integral is similar to the starting one.

The lamp is not the only component which impacts the signal. Optical fibers also play a role. As shown in Figure 11, different curvatures of the fiber modify detector count values. Fiber transparency will determine the usable wavelength range. Fibers connecting the ATR probe to its UV system are transparent enough to analyze compounds with chromophores at about 200−210 nm.

Figure 11. **ATR in air, effect of two different fiber curvatures.**

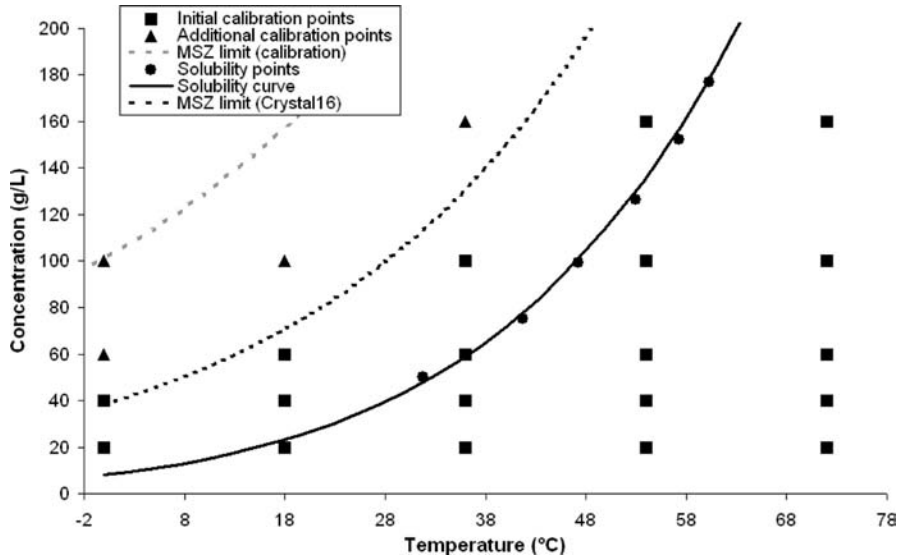

Figure 12. **Calibration points.**

The pixels of the CCD detector are thermally sensitive, which causes a small dark current. To get dynamic correction, the signal of the first 14 pixels of the detector is subtracted from the raw data.

For all of the following work, fiber curvature was kept constant, source stabilization was aquired, and absorbance at peak maximum was corrected from absorbance at 350 nm.

4.3. Calibration. The solubility curve and the MSZW were determined for 6-MNA in ethanol by the Crystal16 system with seven concentrations (25, 50, 75, 100, 125, 150, and to 200 g/L). Results were fitted by a Van't Hoff equation with a coefficient of determination of 0.993 (eq 8 where C is in g/L and T in Kelvin):

$$C = 2.2 \times 10^8 \, e^{-4678.2/T} \qquad (8)$$

These data were necessary to choose calibration points and to establish a model of absorbance as a function of temperature and concentration by a DOE plan. A MSZW of about 16 °C was found, and 19 points were chosen at several concentrations (20, 40, 60; 100, and 160 g/L) and temperatures (0, 18, 36, 54, and 72 °C) for calibration (Figure 12).

The calibration procedure consisted of completely dissolving 6-MNA by heating to 72 °C and then successively cooling the solution to the chosen temperatures. The spectra were recorded between 190 and 400 nm at each 18 °C temperature step, referenced against ethanol at room temperature. The concentration was increased by addition of 6-MNA, and the process was repeated for each new concentration. As cooling rates and agitation conditions were different between the calibration run and the solubility cycles (respectively 0.5 °C/min 700 rpm with a magnetic flea and 5 °C/min with a curved blade turbine) four additional points were obtained beyond the Crystal16

(24) Lewiner, F.; Févotte, G.; Klein, J.; Puel, F. *Chem. Eng. Sci.* **2001**, *56*, 2069.
(25) Mullin, J.; Nývlt, J. *Chem. Eng. Sci.* **1971**, *26*, 369.

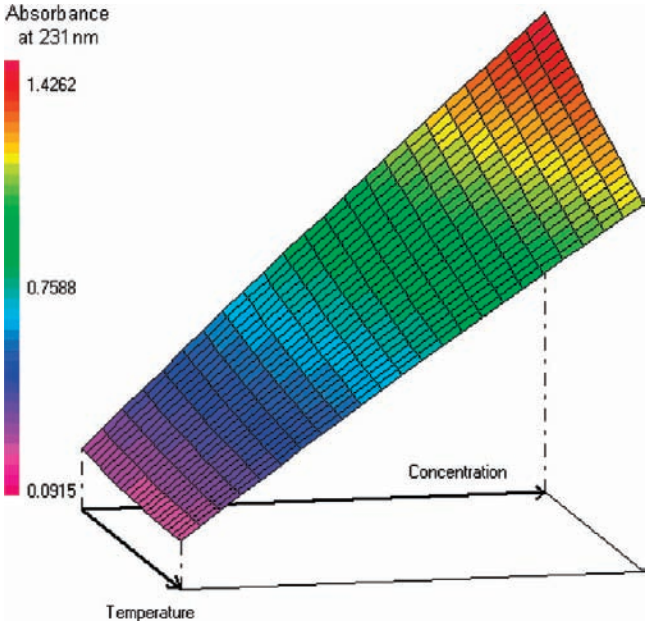

Figure 13. **Three dimensional representation of the calibration model.**

MSZ limit. The calibration MSZW is correspondingly larger (about 39 °C). These additional points fortunately permitted the development of a more robust model, especially for the temperature variable.

The model was the same as Lewiner et al.[24] using the maximum of absorbance at 231 nm as the output of the two variables. Coefficients are given below in eq 9, and Figure 13 shows a three-dimensional representation of the model.

$$\mathrm{Abs} = 4.2541 \times 10^{-2} - 5.1103 \times 10^{-4}T + 8.1211 \times 10^{-6}T^2 + 9.1069 \times 10^{-3}C - 2.8702 \times 10^{-6}C^2 - 2.8286 \times 10^{-5}TC \quad (9)$$

The model has a high accuracy. Observed values against predicted are shown in Figure 14. Four points at concentrations of 30 g/L and 120 g/L, and temperatures of 25 and 60 °C were used to validate the model. Differences between observed and calculated absorbance ranged from 1.4% to 3.2%.

Absorbance is seen to vary in proportion to concentration, in agreement with Beer−Lambert's law, and inversely with temperature, as has been already observed.[8]

4.4. In Situ Measurements during Crystallization. To illustrate the potential of ATR-UV monitoring, temperature, turbidity, and absorbance signals were recorded in real-time during unseeded crystallization processes with two different temperature profiles. The first experiment was performed using the same 0.5 °C/min temperature profile as for determination of solubility curve and MSZW with Crystal16. The second experiment was performed also with a linear temperature profile but at a slower cooling rate of 0.2 °C/min. In a third experiment, a cubic Mullin[25] profile, simplified as a trilinear profile to fit with the cryothermostat limitations, was applied following seeding with 0.5% of milled material (median size about 6 μm) (Figure 15). A heating rate of 0.5 °C/min was conserved for all the experiments.

The raw absorbance signal (Figure 16) shows two maxima which coincide with dissolution and nucleation as detected by turbidimetry. According to the model, maximal absorbance implies simultaneously minimal temperature and maximal concentration, i.e. the lowest temperature at which all the 6-MNA is dissolved. These conditions are met twice during the process, dissolution at heating and nucleation at cooling. These phenomena can be read directly from the raw absorbance signal.

Concentrations calculated from absorbance and temperature measurements using the model eq 9 are shown in Figure 17.

A MSZW of about 22 °C was found for the linear cooling rate of 0.5 °C/min, larger than the value of 16 °C previously measured by Crystal16 but probably a result of different stirring conditions and scale. For all the experiments, the curves in Figure 17 show an excellent fit with the solubility curve. These results show that ATR-UV spectroscopy can be a valuable method to determine solubility curves and MSZW.[9,10]

With a cooling rate of 0.2 °C/min, the return to the solubility curve occurred at a higher temperature. There were, however, no significant differences in MSZW and particle size distribution between the two linear profiles at 0.5 and 0.2 °C/min (Figures

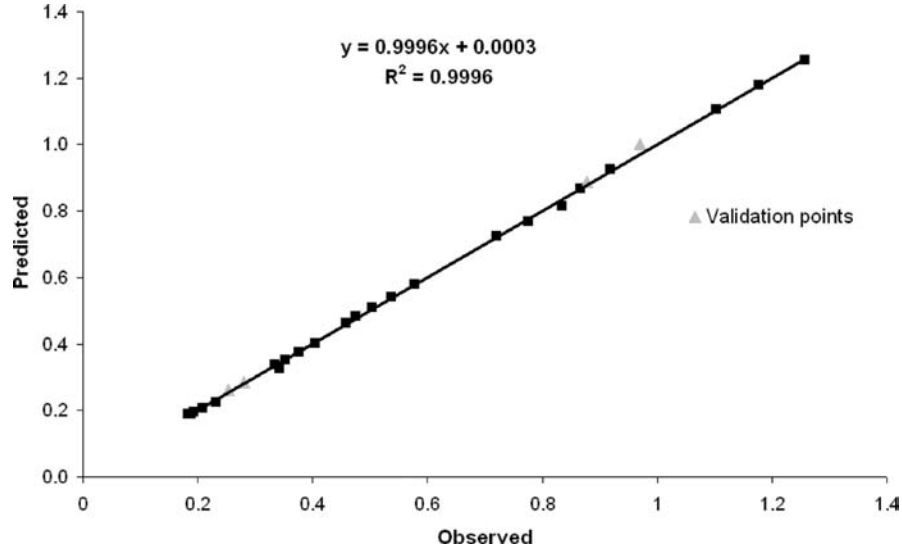

Figure 14. **Observed versus predicted absorbance.**

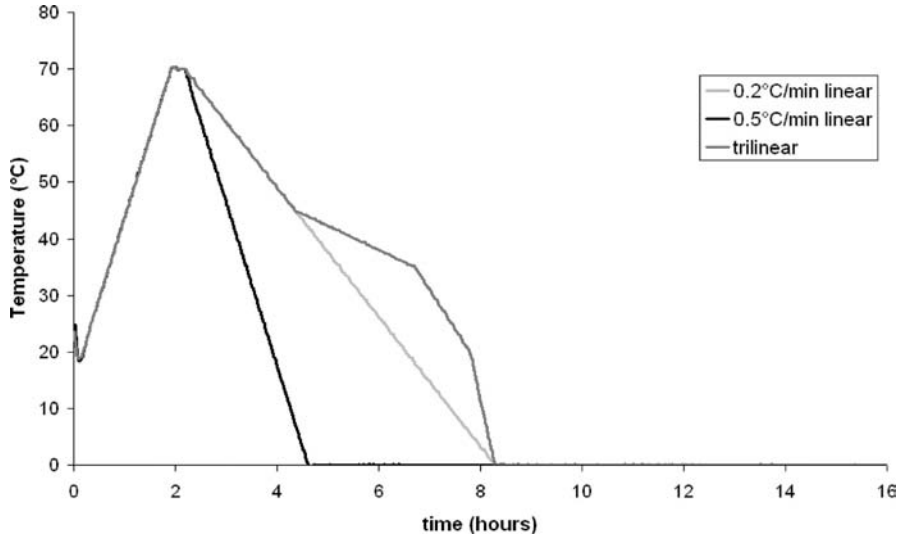

Figure 15. **Temperature profiles used for crystallization processes of 6-MNA 160 g/L in ethanol.**

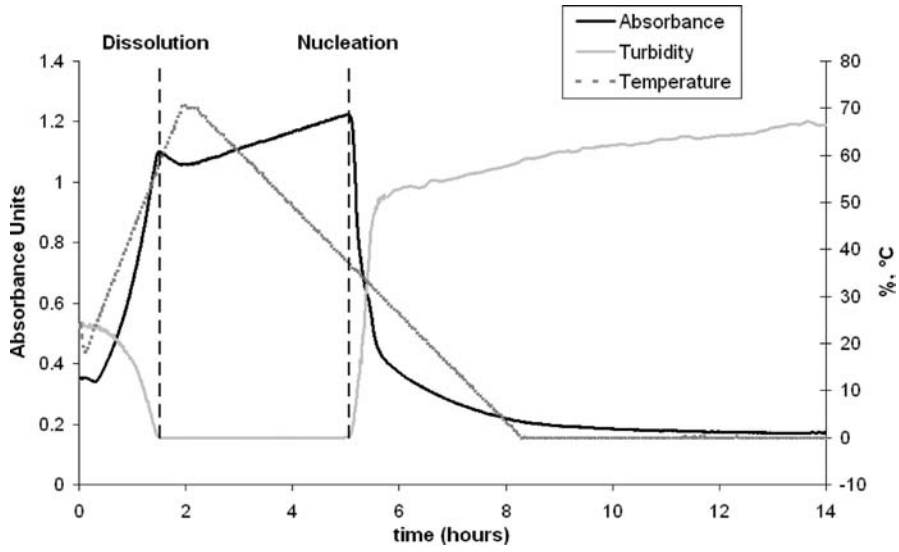

Figure 16. **Real-time measurements of temperature, turbidity, and absorbance during the crystallization process with a cooling rate of 0.2 °C/min.**

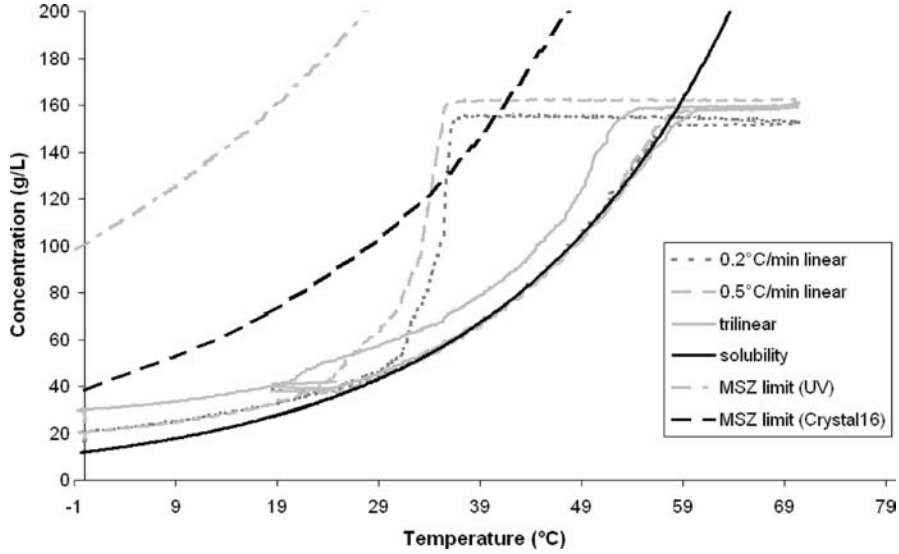

Figure 17. **Evolution of concentration as a function of temperature for linear and trilinear profiles.**

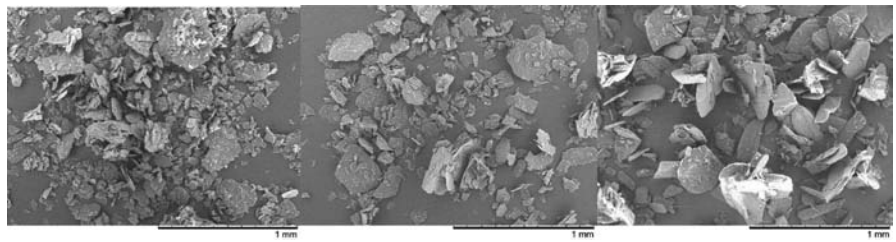

Figure 18. **MEB photos of crystallized 6-MNA using linear profiles at the cooling rates 0.5 and 0.2 °C/min and trilinear profile (from left to right).**

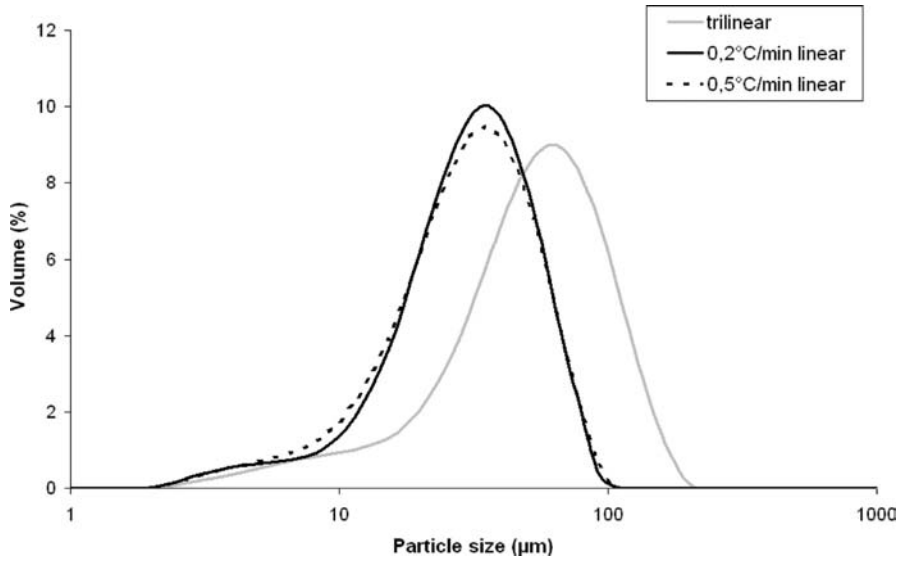

Figure 19. **PSD for linear cooling profiles at 0.5 °C/min and 0.2 °C/min and trilinear profile.**

18 and 19). However, in the case of the trilinear profile the absolute supersaturation remained constant at ∼12 g/L. As constant supersaturation generally makes crystal growth predominate over nucleation, it is not surprising that the particle size distribution resulting from the trilinear profile was on average higher than those resulting from linear profiles.

The experiments cited above and illustrated in Figure 17 show that ATR-UV spectroscopy is an excellent method to monitor solution-phase behavior during the crystallization of UV-absorbing compounds.

4.5. Application to Non-UV-absorbing Substances. As discussed earlier, monitoring the crystallization of nonabsorbing substances by ATR-UV would require that the refractive index of the crystallization system straddle the threshold n_{crit}. The refractive index of the solvent should be close to n_{crit}, the solute and solvent should differ significantly in refractive index, and the solute should crystallize from the solvent. The refractive index would either decrease or increase when crystallizing this substance. For this study, a solvent−substrate system with such characteristics was not identified. Therefore, it was decided to

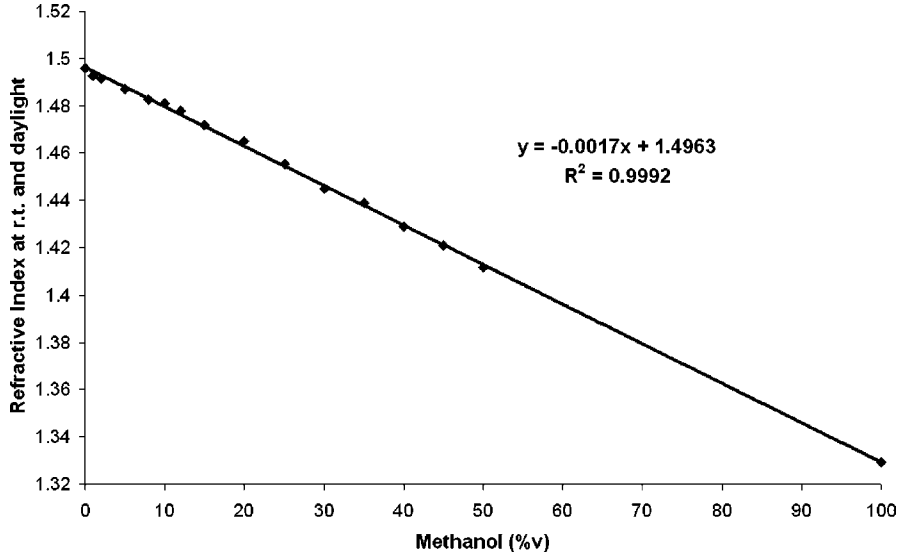

Figure 20. **Linear variation of refractive index of toluene/methanol mixtures with methanol proportion, measured in daylight and room temperature.**

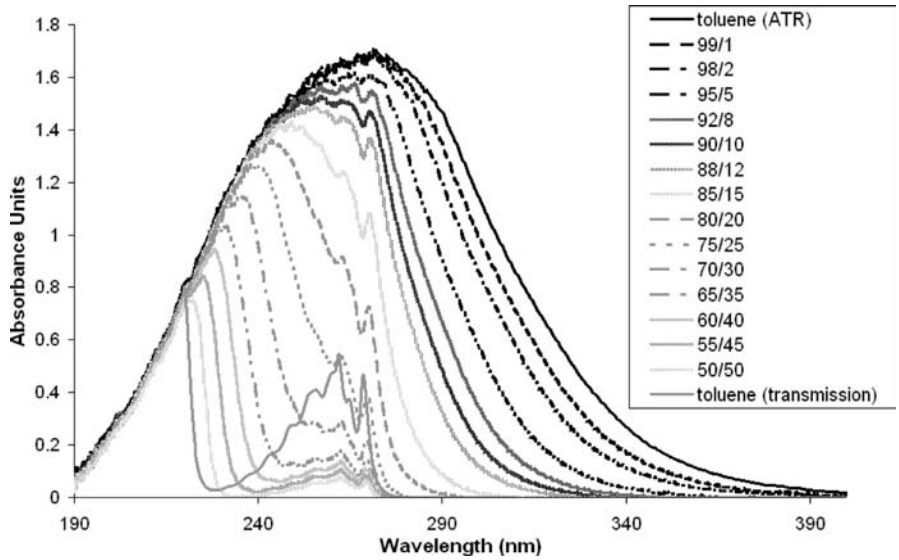

Figure 21. **ATR-UV spectra of the toluene/methanol mixtures and spectrum of toluene in transmission.**

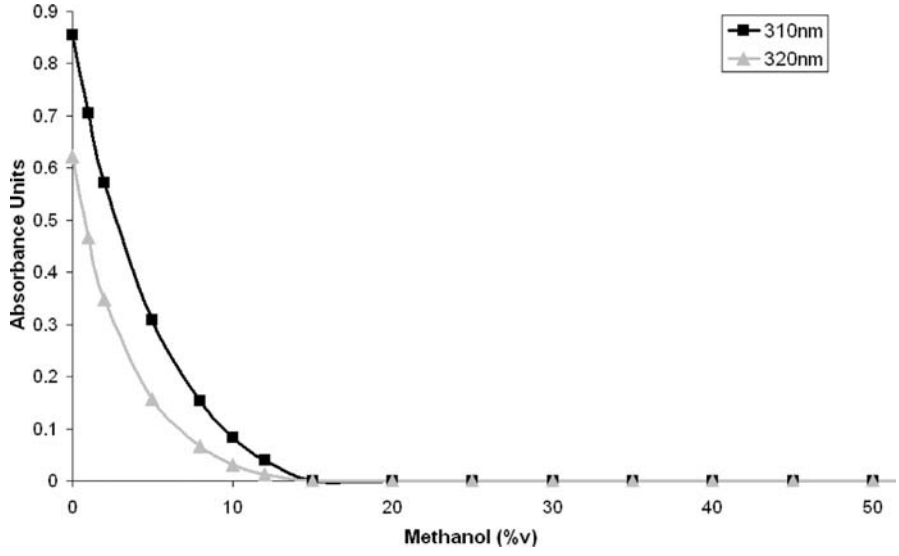

Figure 22. **Calibration curves for absorbance at 310 and 320 nm as a function of methanol proportion.**

demonstrate the feasibility of the analytical aspects of this concept by simulating the variation of refractive index in toluene (refractive index close to n_{crit}, Table 1) by several additions of methanol, a solvent completely transparent in the range studied and with a low refractive index. The refractive index of each mixture was measured in daylight and at room temperature. A linear correspondence of the refractive index to the proportion of methanol (Figure 20) was found.

Spectra of the mixtures were recorded from 190 to 400 nm with air as reference. They are overlaid with the toluene spectrum in transmission in Figure 21.

At concentrations of MeOH in toluene up to 20%, i.e. mixtures with $n \geq 1.4650$, non-null absorbance at wavelengths above 285 nm, where toluene does not absorb, was found. This absorbance decreases when increasing the methanol proportion and thus decreasing the refractive index. At and above 25% methanol (mixtures with $n \leq 1.4554$) the baseline is evident only above 285 nm and peaks at 249 and 256 nm appear that belong to the absorption spectrum of toluene (transmission spectrum as reference).

According to the conclusions drawn from Table 1, when approaching very near to n_{crit}, the effect of the solute on refractive index is more significant than its effect on absorption. At this point, reflection conditions reach the limit between total internal reflection and external reflection. Part of the incident radiation is transmitted into the solution, causing attenuation of the reflected beam independent from potential absorption by sample molecules. The amount of reflected light is significantly reduced and the spectrophotometer registers it as a strong absorption. It is logical that the phenomenon would be less evident when the refractive index deviates from n_{crit}. When the refractive index is decreased far enough from n_{crit}, the effect of absorption predominates over the effect of refractive index, and the spectrum of toluene appears progressively.

Measurements of concentration of nonabsorbing substances would be significant only above the cut-off L_0 of the solvent, i.e., 317 nm for toluene. The wavelengths 310 and 320 nm present significant differences in absorbance. Absorbances at these two wavelengths as a function of methanol proportion are displayed in Figure 22.

This shows that the concentration of nonabsorbing substances can be calculated from real-time measurements of absorbance using a calibration model in the same fashion as for absorbing compounds.

5. Conclusion

Demonstration that ATR-UV spectroscopy, a promising in situ PAT, can be used to monitor the crystallization process of 6-MNA was shown. This technology gives simultaneous access to solubility curve, metastable zone width, and real-time measurements of concentration.

The short optical path length allows direct measurements on strongly absorbing compounds. The lower cut-off wavelengths permit the use of a larger number of solvents than in transmission spectroscopy. Furthermore, even quantitative measurements of nonabsorbing substances are possible through the dependence of internal reflection on the refractive index.

Implementation in an industrial environment is easy and inexpensive, compared with other PAT such as ATR-FTIR. Conformity with ATEX directives is made possible by the use of flexible optic fibers as long as 100 m.

Acknowledgment

We acknowledge Dr. J. R. Authelin, Dr. P. Boffelli and Dr. A. Van Sickle of Sanofi-aventis for fruitful scientific discussions.

Received for review October 30, 2009.

OP900281M